

Size of the Detection Area of a Phase-Doppler Anemometer for Reflecting and Refracting Particles

Frank Schöne, Klaus Bauckhage, Thomas Wriedt*

(Received: 2 December 1992; resubmitted: 3 May 1994)

Abstract

Measurements of particle size distributions in multi-phase flows with a phase-Doppler anemometer yield incorrect results if polydisperse particles are investigated. For weighting biased size distributions, different in situ methods, requiring the size of the detection area, are known, but all of these weighting procedures are restricted to very small measuring volumes if off-axis instrument configurations are considered. Moreover, the weighting functions have some disadvantages in the case of poor statistics in single size classes or the results are not suitable for determining the size of the detection area for particles which are larger than the beam waist.

Therefore, the intention in this work was to measure the size of the detection area for different kinds of monodisperse particles, different instrument configurations and varied instrument sensitivities experimentally and to develop an improved weighting procedure that copes with the above difficulties. The application of the results obtained from the investigations with monodisperse particles to measured particle size distributions and volume flux densities of polydisperse water droplets in a spray cone of an atomizer confirms the applicability of this weighting procedure. It is still restricted to directed flows, perpendicular to the fringes.

1 Introduction

For non-intrusive and simultaneous measurements of particle velocity and particle size, phase-Doppler anemometry is a very suitable method (Bauckhage and Flögel [1], Saffman et al. [2], Bachalo and Houser [3], referring to fundamentals described by Durst and Zaré [4]). This measuring technique yields absolute results of particle size and velocity, but in the case of the prevailing application, i.e. the analysis of multi-phase flows with polydisperse particle collections (Bachalo and Houser [5], Bauckhage [6], Bauckhage et al. [7]), the measured number distributions of particles sizes are biased in a way that large particles are over-represented in comparison with smaller ones ([2], Bauckhage et al. [8], Saffman [9], Bachalo [10]). Therefore, a weighting procedure becomes necessary to obtain correct results for the corresponding distributions and for all related flow parameters, such as particle concentration and mass flux density.

The "size bias" depends on the probability of successful signal processing, which is influenced by the sensitivity of the whole phase-Doppler anemometer (PDA) to individual particle sizes and by the optical characteristics of the spherical particles. The commonly used function for weighting size distributions is the area of detection, being part of the cross-sectional area of the measuring volume. If reflecting particles are measured with the aid of a backscatter PDA, the size of the detection area can be determined very easily (Schöne et al. [11]). Only one parameter, representing the sensitivity of the phase-Doppler instrument and the scattering properties of the particles, is needed. This parameter can be the maximum burst amplitude [2], the mean

value of burst amplitudes (Sommerfeld and Qiu [12]), the maximum burst length, the maximum number of signal periods above a fixed trigger level [8, 10] or the mean value of squared burst lengths [9]. For a specific weighting procedure, either the burst, generated by only one reference particle with well known diameter d_0 , moving through the centre of the measuring volume, or the bursts of single reference particles in each particle size class d_i , have to be analysed with respect to their lengths or amplitudes. Another possibility is to evaluate the bursts of all particles in each size class. These types of (reference) measurements can be performed as a calibration with well known particles of the process fluid [2], which in general is very difficult or may be impossible. The most convenient way is an in situ weighting of the measured number distribution, which was developed in recent years [8-12]. All of these methods and also the method described in this paper are off-line weighting procedures because post-processing of the in situ measurements is required.

In practice, all of these methods show disadvantages or yield incorrect results for the size of the detection area. The weighting functions, which are based on the events in all size classes d_i , may result in errors if single size classes show poor particle statistics as reported by Sommerfeld and Qiu [12]. The other type of weighting procedure, based on only one reference particle in a single size class d_0 , is not applicable if the particles are not much smaller than the beam waist in the measuring volume [11].

While the dependence of the size of the detection area on the burst length could be verified for backscatter arrangements of the transmitting and the receiving optical system with reflecting particles [11], the intention in this work was to investigate the area of detection for off-axis measurements of both reflecting and refracting monodisperse particles. Further, an improved procedure of weighting, requiring a single reference particle,

* Dr.-Ing. F. Schöne, Prof. Dr.-Ing. K. Bauckhage, Dr.-Ing. T. Wriedt, Institut für Werkstofftechnik, Abteilung Verfahrenstechnik, Badgasteiner Str. 3, 28359 Bremen (Federal Republic of Germany).

was applied to particle size distributions, measured in the spray cone of a pressure atomizer, in order to obtain information about the suitability of the investigated weighting function.

2 Area of Detection

2.1 Definitions

The basis of the following explanations is the *interference volume* being generated by the two laser beams of the transmitting system of a conventional laser-Doppler anemometer (LDA) or of a PDA. The spatial shape of this volume can be considered as almost ellipsoidal and the size of the interference volume with N_f fringes is defined by the three $1/e^2$ intensity diameters D_x , D_y and D_z . It differs from the size of the *measuring volume* especially in the case of off-axis configurations, which will only be considered in the following.

Apart from the transmitting optics, generating the interference volume (Figure 1), the size of the measuring volume is influenced by the receiving optics, its aperture and the selected off-axis-angle ϕ . The size of the *detection area*, which is the cross-sectional area of the *effective measuring volume*, depends on the particle size, its optical light scattering characteristics and the instrument sensitivity. The shape of the detection area can nearly be considered as a parallelogram, as can be gathered from Figure 2.

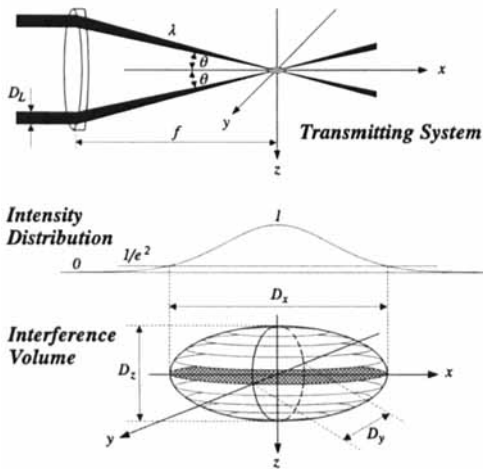


Fig. 1: 2-beam transmitting optic and the ellipsoidal interference volume with a (3-dimensional) Gaussian intensity distribution.

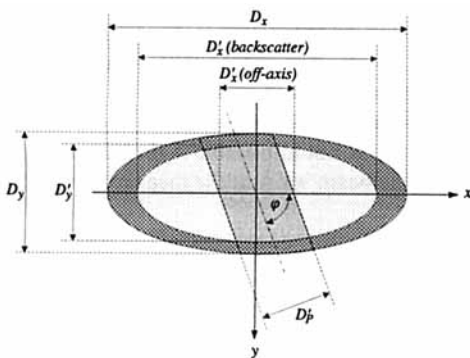


Fig. 2: The area of detection for off-axis instrument configuration as part of the elliptical interference plane in the x - y -coordinate plane.

2.2 Width of the Detection Area

For commonly used off-axis-angles ($30^\circ \leq \phi \leq 150^\circ$), the length D'_x (parallel to the x -axis) of the detection area differs significantly from that of a backscatter instrument and is usually considered as equal to the length $D'_p/\sin\phi$ of the measuring volume (Figure 2), with D'_p being the width of the magnified aperture of the receiving optics.

The width D'_y (parallel to the y -axis) is nearly unaffected, because the receiving optic is able to detect particles in the complete depth of the interference volume but the dependence of D'_y on the particle diameter d must be taken into account. The most important presupposition for the derivation of D'_y is the validity of the laws of geometrical optics, which means that the scattered light intensity I_S is proportional to the incident intensity I_P on the particle and also to the particle diameter squared:

$$I_S \propto I_P d^2 \quad (1)$$

In the case of conventional laser beams with a Gaussian intensity profile (TEM₀₀ mode), the incident intensity depends on the spatial position (x, y, z) of the particle in the interference volume. For particles which are small compared with the diameters of the interference volume, the incident intensity is given by

$$I_P(x, y, z) = I_0 \exp \left[-8 \left(\frac{x^2}{D_x^2} + \frac{y^2}{D_y^2} + \frac{z^2}{D_z^2} \right) \right] \quad (2)$$

where I_0 is the maximum intensity in the centre of the interference volume $x = y = z = 0$. If further the response characteristics of the detectors and amplifiers are considered as being linear, the envelope of the high-pass filtered signal voltage U can be expressed by

$$U(d, x, y, z) = C d^2 \exp \left[-8 \left(\frac{x^2}{D_x^2} + \frac{y^2}{D_y^2} + \frac{z^2}{D_z^2} \right) \right] \quad (3)$$

where C is a constant. For the validity of this equation, the signal visibility must be assumed to be close to unity, because otherwise the amplitude of the high-pass filtered signal, the AC part of the signal, is not proportional to the particle diameter squared. For such occasions, the pedestal of the burst can be evaluated by means of a more extensive signal processing system.

Substituting the length ratio z/D_z in Eq. (3) by a fringe ratio f/N_f yields

$$U(d, x, y, f) = C d^2 \exp \left[-8 \left(\frac{x^2}{D_x^2} + \frac{y^2}{D_y^2} + \frac{f^2}{N_f^2} \right) \right] \quad (4)$$

Using a counter processor for signal processing, the burst detection is commonly done by means of a trigger level U_t which must be exceeded by the signal voltage. For signal validation the filtered AC signal has to exceed the trigger level with at least N_{\min} periods. In the case of particle trajectories, crossing the y -coordinate axis perpendicular to the fringes, this condition can be expressed by introducing the maximum trajectory displacement into Eq. (4). This maximum possible displacement along the y -coordinate axis is given by half of the width $D'_y/2$ of the detection area:

$$\begin{aligned} U_t &= U(d, x = 0, y = D'_y(d)/2, f = N_{\min}/2) = \\ &= C d^2 \exp \left[-2 \left(\frac{D'_y(d)^2}{D_y^2} + \frac{N_{\min}^2}{N_f^2} \right) \right] \end{aligned} \quad (5)$$

All particles with diameter d , crossing the interference volume on the z -axis, will generate the maximum possible number of periods $N_{\max}(d)$. This results in another equation for the trigger level:

$$U_t = U(d, x = 0, y = 0, f = N_{\max}(d)/2) = C d^2 \exp\left[-2 \frac{N_{\max}^2(d)}{N_f^2}\right]. \tag{6}$$

Equating Eq. (5) and Eq. (6) for the fixed trigger level yield

$$D'_y(d) = D_y \sqrt{\frac{N_{\max}^2(d) - N_{\min}^2}{N_f^2}}. \tag{7}$$

This result can be used to calculate the particle size-dependent width of the detection area. For this it is necessary to determine the maximum possible number of burst periods in each size class d_i of the measured particle size distribution. In the case of poor statistics in those size classes at the lower and especially at the upper end of the measured size distribution, the probability of detecting signals with the maximum possible number of periods is very low. This disadvantage also occurs if the in situ determination is based on mean values for the burst length or for the burst amplitudes.

In order to avoid errors resulting from poor statistics, the size class with the maximum number of particles is defined as a reference size class. In this special size class that particle with diameter d_0 having generated the maximum number of periods $N_{\max}(d_0) = N_0$ is defined as a reference particle for the whole particle collection actually measured. With these in situ measurement results a further equation, analogous to Eq. (6) for the trigger level, can be derived. After equating the result

$$N_{\max}^2(d) = N_{\max}^2(d_0) + N_f^2 \ln \frac{d}{d_0} \tag{8}$$

can be used to substitute the term $N_{\max}(d)$ in Eq. (7), resulting in

$$D'_y(d) = D_y \sqrt{\ln \frac{d}{d_0} + \frac{N_0^2 - N_{\min}^2}{N_f^2}}. \tag{9}$$

As mentioned above, one important presupposition for the applicability of Eq. (9) is the validity of the laws of geometrical optics, which means that the scattered light intensity is proportional to the particle diameter squared ($I_s \propto d^2$). In the interference volume with its Gaussian intensity distribution this is only accomplished if the particle diameter is very small in comparison with the diameters $D_y \cong D_z$ of the interference volume. In the case of broad particle size distributions this generally cannot be achieved for all particles.

In order to consider the fact that the extension of the interference volume is limited, the scattered intensity has also to be regarded as limited, because the particle cannot scatter more light than that one of the incident laser beams. Consequently, extended theoretical considerations must be based on the ratio of particle diameter d and a characteristic diameter of the interference volume, e.g. the width D_y of the interference volume.

With the intention of not requiring extensive numerical calculations according to the (generalized Lorenz-) Mie theory (Gréhan et al. [13]) a simple formalism could be derived which is based on a geometrical model describing the scattered power of light. For the corresponding derivation, the incident power $P_P(d)$ on the particle, situated in the centre of the interference volume,

which has a circular shape in the y - z -coordinate plane ($D_y \cong D_z$), is calculated:

$$P_P(d) = \int_0^{d/2} I(r) 2\pi r dr = \int_0^{d/2} I_0 \exp\left(-8 \frac{r^2}{D_y^2}\right) 2\pi r dr = \dots = \frac{\pi I_0 D_y^2}{8} \left[1 - \exp\left(-2 \frac{d^2}{D_y^2}\right)\right]. \tag{10}$$

If further the approximation is introduced that the incident power on the particle results from a complete Gaussian intensity distribution, comparable to that of a laser beam with a circular cross-section

$$P_P(d) = \int_0^\infty I(r) 2\pi r dr = \int_0^\infty I_0(d) \exp\left(-8 \frac{r^2}{D_y^2}\right) 2\pi r dr = \dots = \frac{\pi D_y^2}{8} I_0(d) \tag{11}$$

the incident power is proportional to the central intensity $I_0(d)$, which now depends on the particle diameter. After combining Eq. (10) and Eq. (11) the resulting equation:

$$I_0(d) \propto 1 - \exp\left(-2 \frac{d^2}{D_y^2}\right) \tag{12}$$

can be used to substitute I_0 in Eq. (2) and the signal amplitude $C d^2$ in Eq. (3):

$$U(d, x, y, z) = C_1 \left[1 - \exp\left(-2 \frac{d^2}{D_y^2}\right)\right] \exp\left[-8 \left(\frac{x^2}{D_x^2} + \frac{y^2}{D_y^2} + \frac{z^2}{D_z^2}\right)\right] \tag{13}$$

where C_1 is a constant. Analogously to Eq. (6), the trigger level U_t can be expressed by means of the in situ measurement results ($d_0, N_{\max}(d_0)$) of the reference particle and also with the corresponding results for each other particle of the size distribution:

$$U_t = C_1 \left[1 - \exp\left(-2 \frac{d^2}{D_y^2}\right)\right] \exp\left[-2 \left(\frac{N_{\max}^2(d)}{N_f^2}\right)\right] = C_1 \left[1 - \exp\left(-2 \frac{d_0^2}{D_y^2}\right)\right] \exp\left[-2 \left(\frac{N_{\max}^2(d_0)}{N_f^2}\right)\right]. \tag{14}$$

The same formalism, leading to Eq. (8) and Eq. (9), now results in the following improved equations for the maximum number of burst periods:

$$N_{\max}^2(d) = N_{\max}^2(d_0) + \frac{1}{2} N_f^2 \ln \left[\frac{1 - \exp\left(-2 \frac{d^2}{D_y^2}\right)}{1 - \exp\left(-2 \frac{d_0^2}{D_y^2}\right)} \right] \tag{15}$$

and for the width of the detection area, depending on the in situ measurement results from a reference particle:

$$D'_y(d) = D_y \sqrt{\frac{1}{2} \ln \left[\frac{1 - \exp\left(-2 \frac{d^2}{D_y^2}\right)}{1 - \exp\left(-2 \frac{d_0^2}{D_y^2}\right)} \right] + \frac{N_0^2 - N_{\min}^2}{N_f^2}}. \tag{16}$$

Although by this formalism the trajectory-dependent effects on the signal amplitude and phase, discussed by Gréhan et al. [13] and Sankar et al. [14], were not taken into consideration, the results achieved warrant the choice of this geometrical model, because it is suitable for describing the limiting effects of the scattered intensity and of the width of the detection area. In Figure 3 it is shown that the scattered intensity underlying this result (case B) differs from the parabolic curve (case A), which

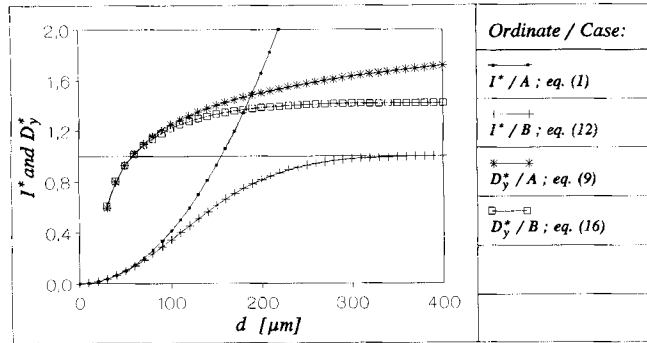


Fig. 3: Normalized scattered light intensity I^* and normalized width $D'_y (=D'_y/D_y)$ of the detection area depending on the particle diameter for two different cases:

A) Illumination of the particle by a beam of infinite extensions and a uniform intensity distribution and
B) by a beam with Gaussian intensity profile and circular cross section (diameter D_y).

D'_y are calculated with the values: $D_y = 217,8 \mu\text{m}$, $N_f = 26,4$, $N_{\min} = 5$, $d_0 = 50 \mu\text{m}$, $N_0 = 25$. The intensity normalization is done in two steps: first for curve B, the intensity for the maximum particle diameter considered, was defined as unity: $I(d_{\max} = 400 \mu\text{m}) = 1$. For curve A the results were subsequently rescaled in a way that for both cases the intensities at the particle diameter d_0 became equal.

is the basis for Eq. (9). Further, in Figure 3 it is shown that the width of the detection area is also limited and it is smaller than that obtained from Eq. (9). In the case of small particles ($d \ll D'_y$), the corresponding curves become equal, as expected. If monodisperse particles ($d = d_0$) are to be investigated, Eqs. (9) and (16) can be reduced to the simple equation

$$D'_y = D_y \sqrt{\frac{N_0^2 - N_{\min}^2}{N_f^2}} \quad (17)$$

which only requires the measurement of the maximum number N_0 of signal periods. Moreover, these results are still restricted to particles with trajectories perpendicular to the interference planes, which will only be considered in the following. Another limitation is that frequency offsets are neglected, but the enlargement or reduction of the diameter D'_y due to this additional instrument parameter can easily be taken into account by introducing the number N_s of additional burst periods caused by a frequency shift:

$$N_0 = N_b - N_s = N_b - N_b \frac{f_s}{f_b} = N_b \frac{f_b - f_s}{f_b} \quad (18)$$

where N_b = total number of burst periods, f_b = frequency of burst and f_s = shift frequency.

On the premises that the diameter d_0 of the reference particle is small compared with the diameter D_y ($d_0 \ll D_y$), for Eq. (9) and also approximately for Eq. (16), the lower limit d_{\min} of particle sizes is given by

$$d > d_{\min} = d_0 \exp\left(-\frac{N_0^2 - N_{\min}^2}{N_f^2}\right). \quad (19)$$

This minimum diameter represents the smallest particle which can be detected by the phase-Doppler anemometer, operating at the selected instrument sensitivity. But this, d_{\min} is a specific sensitivity parameter, being influenced by the in situ calibration measurement of d_0 and N_0 .

2.3 Length of the Detection Area

In several publications [9, 10, 12], the length D'_x of the detection area is regarded as being constant, depending only on the instrument parameters and not on the particle diameter or other parameters. The presupposition for this assumption is that the length of the detection area is small in comparison with the corresponding length of the interference volume ($D'_x \ll D_x$). Even if the instrument parameters meet this condition, which means that the constant length $D'_p/\sin\phi$ of the pinhole or slit projection of the receiving system is smaller than 5% of the diameter D_x , errors due to blurring in the receiving optics are reported [9, 10, 15]. The blurring is characterized as being dependent on the particle diameter in addition to enlarging the length of the detection area. Further, experimental results will show that the length of the detection area depends on the instrumental sensitivity and on the particle diameter. For this reason, in the following D'_x is not considered as constant. This becomes very important for applications with long working distances. In these cases it cannot be guaranteed that the length of the detection area is very small in comparison with the corresponding diameter of the interference volume.

Owing to the similar appearance of the period distributions, measured along the x -coordinate axis and along the y -axis, within the length $D'_p/\sin\phi$ an almost elliptical shape of the fringe distribution in the x - z -coordinate plane could be assumed as is given for the y - z -plane. This empirical result of extensive experimental investigations yields the following equation for the length of the detection area:

$$D'_x = \frac{D'_p}{\sin\phi} \sqrt{\ln \frac{d}{d_0} + \frac{N_0^2 - N_{\min}^2}{N_f^2}} + \frac{d}{2}. \quad (20)$$

This equation is similar to Eq. (9) describing the width of the detection area because of almost identical assumptions. The additional term $d/2$ was introduced in order to give a more reliable fitting of this equation with the experimental results (Sections 4.1.3 and 4.1.4). Both an enlargement (probably caused by blurring) and a reduction (probably due to cut-off effects) will be described by Eq. (20). The amount of variation with respect to the length of the measuring volume ($D'_p/\sin\phi$) depends on the measured results (d_0 , N_0) for the reference particle.

The lack of physics in connection with Eq. (20) is the subject of further studies. Following the investigations performed by Sellens [16], ray-tracing simulation experiments seem to be a suitable method for describing the cut-off effects at the slit aperture in the receiving optics with its finite width. This cut-off results from particle trajectories crossing the detection area outside the centre. The consequence of non central trajectories is demonstrated in Figure 4. The two photographs show the scattered light (fringe) pattern behind the slit aperture in the receiving optics. Obviously, the displacement of the particle (trajectory) only the x -coordinate axis results in a loss of detectable light intensity and power. This indication also confirms the decrease of measured burst periods depending qualitatively on the displacement as is shown in Figure 4.

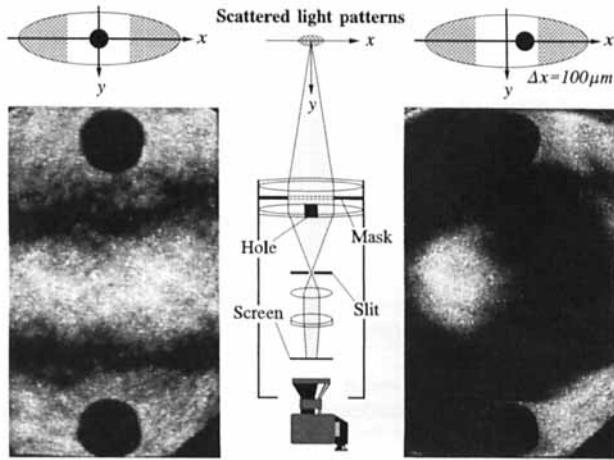


Fig. 4: Parts of the scattered light pattern generated by a stationary steel bead ($d = 300 \mu\text{m}$) and photographed in the APD receiving optics behind the mask and the slit aperture. For these photos the detector assembly was substituted by a screen and a camera and a mask with a single rectangular aperture, mounted perpendicular to the fringes was selected. The black circles were caused by holes in one lens, enabling backscatter configurations. For the present off-axis measurements these holes did not be visible because another mask was used.

Left photo: The steel bead is situated in the centre of the measuring volume.

Right photo: The steel bead is situated $100 \mu\text{m}$ beside the centre of the measuring volume.

3 Experiments

3.1 Experimental Procedure

3.1.1 Monodisperse Particles

In order to verify the theoretical results and assumptions by experimental investigations with monodisperse particles ($d = d_0$), the most important parameter to be measured is the maximum number N_0 of burst periods produced by a particle crossing the measuring volume in its centre perpendicular to the fringes. The diameters D'_x and D'_y , resulting from this “period evaluation” will be compared with the results of a comparative measurement. The basis of these experiments is to scan the moving particles through the measuring volume and in its vicinity to find the boundaries of the detection area by something like a trial-and-error of signal processing. Each of the regularly spaced positions in a predefined rectangular area, where phase-Doppler measurements were executed successfully, was defined as inside the detection area and all positions where the validation rate was less than 5%, referred to 100 attempts, were defined as outside the detection area. After the reconstruction of the detection area with the aid of those positions where the phase-Doppler measurements were successfully, the wanted diameters D'_x and D'_y could be determined. This “scan evaluation” and the other type of evaluation, the “period evaluation”, were executed simultaneously, because the parameter N_0 could be determined from the same dataset. The maximum number of signal periods had to be searched in the centre of the detection area.

The measurements were carried out with different settings of the electronic amplification V and attenuation $V^* = -V$, with different off-axis angles φ and different types of particles and particle diameters.

3.1.2 Polydisperse Particles

In the experimental investigations with polydisperse particles, a broad size spectrum of water droplets was generated by a pressure atomizer within a spray chamber. For this type of experiment the accuracy of the weighting procedure was analysed by comparing both the weighted number distributions and the calculated volume flux densities, which were measured at different off-axis locations of the receiving system. Further, the volume flux densities could be referred to patternator measurement results, obtained just after the phase-Doppler measurements and 1 mm below the interference volume.

3.2 Experimental Set-up

For the experimental investigations, a conventional two-beam LDA transmitting system with an He-Ne laser ($\lambda = 632.8 \text{ nm}$) was used and the detection of the scattered light was done by means of a laboratory-made receiving optical system with two integrated Avalanche photodiodes (APD receiver). The spatial filter in the receiving system is equipped with a slit aperture (width $D_p = 200 \mu\text{m}$, length 3 mm), which is oriented perpendicular to the area of detection.

For some additional experiments, requiring a variable length of the measuring volume, a conventional receiving system, consisting of a photomultiplier and a zoom objective, was used. The dimension of the pinhole aperture in this PM receiver was specified as $D_p = 100 \mu\text{m}$. In order to avoid any errors caused by a non-ideal alignment of two receivers, these experiments, performed on monodisperse particles, were conducted with only one PM receiver. By this means the particle diameter could not be measured with the PDA, which was not necessary because the sizes of the monodisperse particles were well known. Only the maximum number of signal periods had to be measured.

The size range for the different particles under investigation could be adapted by varying the beam separation in the transmitting system and by changing the front lens in the receiving system. The most important instrument parameters are listed in the Table 1 with respect to the different applications and particles respectively (steel bead, water droplets and spray of water).

In all cases the signal processing was performed by means of a counter processor, because this was a device capable of measuring the signal frequency and the phase difference and also the burst length by counting the number of periods.

3.3 Characteristics of the Monodisperse Particles

In order to investigate the dependence of the detection area on the scattering characteristics (reflection or refraction), two different types of particles were used. In both cases the trajectories of the moving particles were aligned perpendicular to the fringes.

3.3.1 Steel Bead

Similarly to the experimental procedures performed by Naqwi et al. [18], a polished steel bead, welded on top of a needle, was fixed to a rotating disc. The steel bead was used as a reflecting specimen. Its diameter was $300 \mu\text{m}$ and could be measured by means of microscopic investigations.

Table 1: Calculated parameters of the phase-Doppler instrument selected for different applications. The beam diameter was measured by means of a "Beam Scan" device.

Parameter	Steel bead	Water droplets	Steel bead and spray
	Transmitting system		
λ	632.8 nm	632.8 nm	632.8 nm
Beam diameter	2.22 mm	2.22 mm	2.22 mm
Beam separation	46 mm	35.6 mm	46 mm
Focal length	1200 mm	600 mm	600 mm
D_x	22726.8 μm	7341.3 μm	5684.8 μm
D_y	435.5 μm	217.8 μm	217.8 μm
D_z	435.6 μm	217.9 μm	217.9 μm
N_f	26.4	20.4	26.4
Receiving system			
Aperture of spacial filter	Pinhole \varnothing 100 μm	Slit 200 $\mu\text{m} \times 3$ mm	Slit 200 $\mu\text{m} \times 3$ mm
Aperture of mask	circular 48 mm	rectangular 60 mm \times 10 mm	rectangular 60 mm \times 10 mm
Detector separation	—	33.4 mm	33.4 mm
Focal length to spacial filter	100 mm	160 mm	160 mm
Focal length to interference volume	600...1000 mm	501 mm	1001 mm
Off-axis angle	30°, 60°, 90°	30°, 60°, 90°	30°, 60°
D'_p	600-1000 μm	626.0 μm	1249.8 μm

3.3.2 Water Droplets

If water droplets with a refractive index $n_d = 1.33$ are investigated at off-axis angles of $\varphi = 30^\circ$ and 60° with light polarized parallel to the interference fringes, *refraction* is the dominant scattering mechanism (Manasse et al. [17]). Water droplets can also be used as a reflecting specimen. For this it is necessary to vary the off-axis angle and also the direction of polarization in order to obtain a linear relationship between droplet diameter and phase difference. A suitable choice is an instrument configuration with $\varphi = 90^\circ$ polarization perpendicular to the interference fringes.

This can be checked by means of numerical light scattering computations according to the Mie theory. The results of such simulations performed for those instrument parameters (Table 1) which were selected for the measurements on water droplets from a droplet generator are shown in Figure 5. Apart from the fact that in the range of small particles some oscillations occur, the different curves can be considered as being linear and in good agreement with the results of geometrical optics.

Droplets with four different diameters in the range of about $55 \mu\text{m} \leq d \leq 190 \mu\text{m}$ were generated by a piezoelectric droplet generator with a repetition rate of about 40 kHz up to 60 kHz. Both the diameters and the trajectories of the water droplets could be observed with the aid of a microscope and stroboscopic illumination.

3.4 Positioning

The three-dimensional alignment and the horizontal movement of the rotating disc and the droplet generator, parallel to the interference planes, could be performed by means of three-dimen-

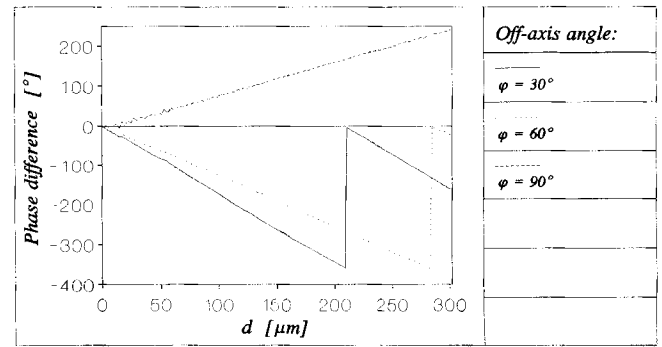


Fig. 5: Phase difference versus particle diameter as a result of numerical computations according to the Mie theory for that PDA to be applied to water droplets from the piezoelectric droplet generator.

sional stepper motor-driven translation stages. By this means the particles were moved to predefined positions within rectangular areas (Figure 6).

While the steel bead could be scanned through a large area with the complete detection area inside, the scan procedure for the water droplets had to be modified because of the non-stationary state of the droplet generator. For shortening the measuring time the water droplets were scanned only within a small area in the centre and at the boundaries of the detection area to obtain both the maximum number N_0 of signal periods (in the centre) and the diameters D'_x and D'_y , which are the maximum distances parallel to the corresponding coordinate axis between those positions where measurements were possible (opposite borders).

The constant interval lengths parallel to the x - and the y -coordinate axes were defined in such a way that the scan area was subdivided into 40-60 intervals along each coordinate axis, resulting in 1600-3600 positions for the investigations with the steel bead. In the case of monodisperse water droplets each of the five small scan areas consisted of 25-50 positions.

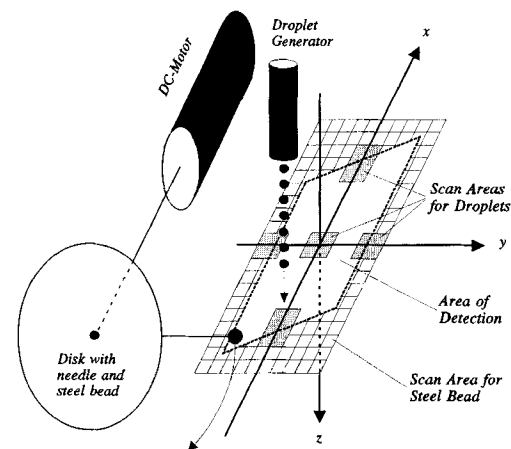


Fig. 6: Principle of positioning the monodisperse particles to regularly spaced positions within one large (steel bead) or several small (water droplets) predefined rectangular areas in the x - y -coordinate plane.

3.5 Atomization

The atomization of water was done by means of a pressure nozzle (Spraying Systems: SS 650050), mounted in the centre of a spray chamber and operated at a pressures of 5 bar. Here, the description of the nozzle, the spray cone and the chamber with

all necessary equipment and features can be omitted, as it has been covered in numerous publications, e.g. Dannehl and Schulte [19].

With the intention of guaranteeing particle trajectories, being perpendicular to the interference planes, the phase-Doppler interference volume was positioned in the centre of the spray cone. The vertical distance to the well known nozzle was set to 200 mm, because at this location the maximum number of small droplets can be detected [7], which was important for applying the weighting function to a broad particle size distribution.

For these experiments some instrument parameters had to be changed (Table 1) while not influencing its applicability, as confirmed by corresponding Mie calculations (Figure 7).

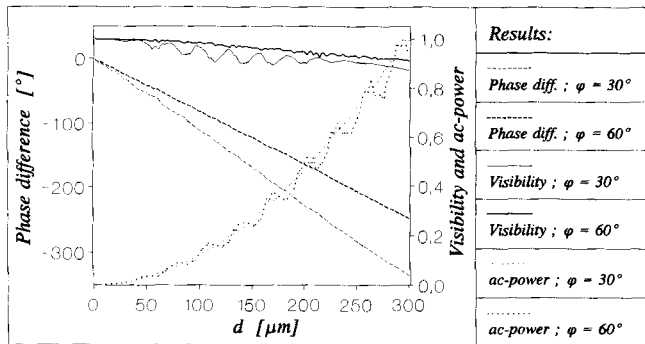


Fig. 7: Phase difference, signal visibility and normalized AC-power versus particle diameter as a result of numerical computations according to the Mie theory for that PDA to be applied to water droplets from the atomizer. The normalization of the AC-power was performed by means of the maximum value of each curve within the plotted size range.

The diameter-phase difference correlation is still monotonic and nearly linear. Apart from that, the visibility, being assumed to be close to unity, in fact shows only small deviations within the particle size range of interest ($0 < d \leq 220 \mu\text{m}$) which are almost completely within a 10% margin. Further, if the Mie calculations are based on an infinite diameter of the incident laser beam, the (normalized) AC power of the detected signal is nearly a parabolic curve, as expected for high visibilities.

4 Results

4.1 Monodisperse Particles

4.1.1 Y-coordinate, Reflection

The results concerning the width D'_y of the detection area, measured with a single, light-reflecting steel bead having a diameter of $300 \mu\text{m}$, are shown in Figure 8. For both off-axis angles ($\varphi = 30^\circ$ and 60°) the corresponding curves have the expected characteristic.

Increasing attenuation V^* , which is equivalent to decreasing instrument sensitivity, yields lower diameters D'_y of the detection area. Apart from this, the measured “scan” results are very well represented by the calculated diameters according to Eq. (17), which are indicated as “period” results. The maximum deviations between the scan and the period evaluations are smaller than 4% for all selected attenuations and both off-axis angles. Similarly to former investigations with a backscatter-PDA [11], the results of the different types of evaluation are in very good

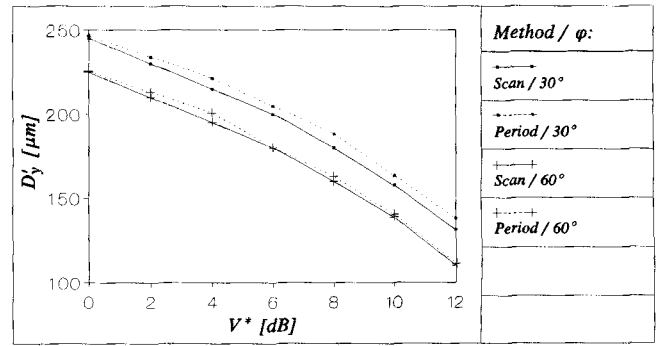


Fig. 8: Width D'_y of the detection area versus electrical attenuation V^* for two types of evaluation (scan- and period evaluation) and two off-axis angles ($\varphi = 30^\circ$ and 60°). The measurements were performed with a steel bead and the APD-receiver.

agreement, so that the burst length method and the period method can also be considered as suitable for the in situ determination of the width of the detection area.

In the case of $\varphi = 90^\circ$ off-axis measurements at transparent water droplets, light reflection is also the dominant scattering mechanism. Some results of such measurements, conducted with a constant instrument sensitivity, are shown in Figure 9. In this diagram the width of the detection area is plotted against the diameter of the droplets. In addition to the previously discussed period evaluation according to Eq. (17) for monodisperse particles, the dependence of the width D'_y of the detection area on the particle diameter d was calculated with the aid of the results ($d_0; N_0$) of a reference measurement by Eq. (9) and Eq. (16). The measurement with the smallest droplets was defined as the required reference measurement.

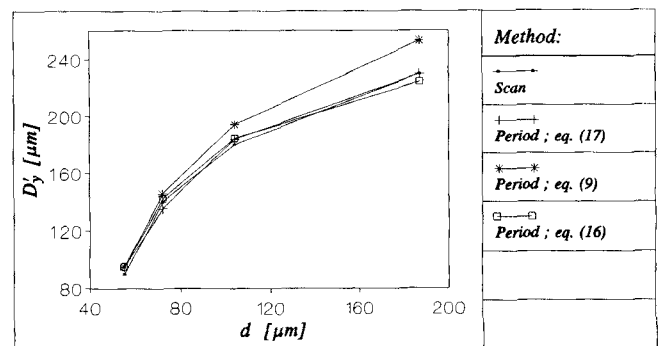


Fig. 9: Width D'_y of the detection area in dependence on the diameter d of reflecting water droplets as a result of the scan measurements and different types of period evaluation. The measurements were performed with the APD-receiver at $\varphi = 90^\circ$.

Just as the period evaluation based on Eq. (9) failed in connection with backscatter measurements on steel beads with different diameters [11], this method is also not well suited for the in situ determination of the width D'_y of the detection area in the case of off-axis configurations. In contrast to the results with Eq. (16), the deviations from the scan results become larger with increasing particle diameter. This is also expressed by the corresponding curves in Figure 3.

Based on the good agreement of the results of the improved period method with the scan results, the applicability of this period method is also confirmed for investigations with (polydisperse) particles of different sizes.

4.1.2 Y-coordinate, Refraction

As one example of this type of experimental investigation, the results of several 30° off-axis measurements with water droplets are illustrated in Figure 10.

The curves for the different methods of evaluation show the same characteristics as the corresponding ones for $\varphi = 90^\circ$ measurements, the deviations being only of a quantitative kind. The results of all types of period evaluation differ from the scan results more than before. Errors or deviations between the preferred period method and the scan results with a magnitude of up to 10% can be registered at small particle diameters, but these differences may be caused exclusively by erroneous period counting as will be discussed in one of the following sections. The important inference is that no significant difference between the results from reflecting and refracting particles could be ascertained.

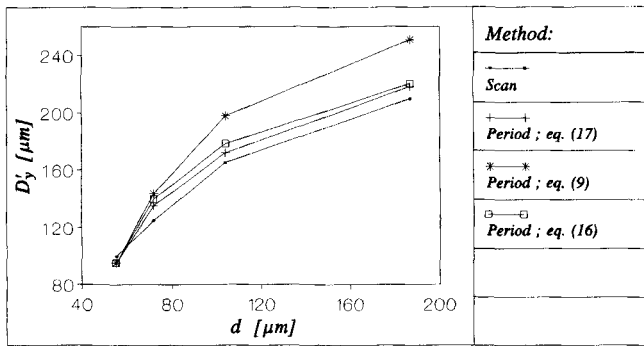


Fig. 10: D_y' of the detection area in dependence on the diameter d of refracting water droplets as a result of the scan measurements and different types of period evaluation. The measurements were performed with the APD-receiver at $\varphi = 30^\circ$.

4.1.3 X-coordinate, Reflection

The empirical determination of the length D_x' of the detection area according to Eq. (20) was done by means of the distributions of the maximum burst periods N_{max} in the detection area, especially along the x -coordinate axis, measured with a 90° off-axis PDA. In Figure 11 a typical example of a period distribution as a result of scan measurement on a steel bead is shown. Although the geometrical and optical parameters of the phase-Doppler instrument were set in such a way that the length D_p' of the measuring volume was only 4% of the length of the

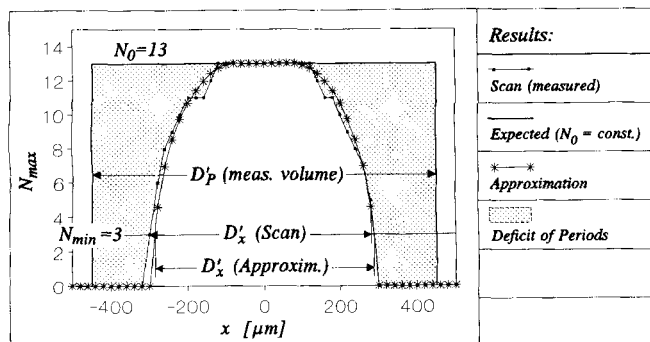


Fig. 11: Comparison of the maximum measured and approximated number of burst periods along the x -coordinate axis for one measurement at the steel bead with only one PM-receiver ($\varphi = 90^\circ$, $f_v = 600$ mm). As against to the expected, almost constant period distribution the scan results show the figured deficits.

interference volume ($D_x = 22727 \mu\text{m}$), the measured number of burst periods is not constant as assumed by other workers [9, 10, 12]. This also happens if much smaller particles (e.g. water droplets about 55 μm in diameter) than the steel bead are investigated.

At the borders of the detection area the measured period distribution shows large deficits in comparison with the expected, constant distribution along the x -axis. One effect of this is that the length of the detection area differs from the length of the measuring volume. Therefore, the length of the detection area cannot be considered either as constant or as equivalent to the length of the measuring volume. Further, these deficits cause erroneous determination of the width of the detection area if the weighting function is based on mean values of burst amplitudes or burst lengths.

Similarly to the width of the detection area, its length also has to be approximated in order to develop a more precise weighting procedure not requiring a calibration. In the range of the parameter N_{min} of interest which is commonly set to $3 \leq N_{min} \leq 8$, the measured period distribution can be approximated by the function of an ellipse, being "stretched" in the centre by an amount $d/2$ as is also shown in Figure 11. The approximate length can be determined by means of Eq. (20). This means that the distances between the two intersection points of the line N_{min} with the curve representing the approximate period distribution are calculated. Therefore, the corresponding "scan" result is given by the maximum distance along the x -axis between those points where validated bursts could be obtained. In Figure 12, this type of approximation, which leads to the

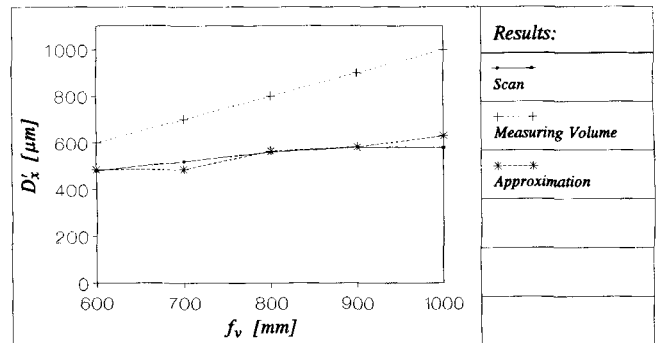


Fig. 12: Length D_x' of the detection area versus the distance (focal length) f_v of a single PM-receiver ($\varphi = 90^\circ$, steel bead). The results of the scan measurement and the approximation are compared to the length of the measuring volume.

hypothesis of Eq. (20), is extended to measurements with increased and decreased lengths of the measuring volume and varied focal lengths of the receiving system. The results of the scan evaluation and the approximation are still in good agreement, even though instrument sensitivity was changed, which was necessary in order to avoid saturation of the photomultiplier especially at short working distances (small focal lengths). The graph in Figure 12 also confirms the very large deviations between the length of the measuring volume and the length of the area of detection. This even happened although the maximum ratio D_p'/D_x did not exceed the value of 0.044 ($f_v = 1000$ mm).

If the reflected light from the steel bead is detected at off-axis angles of $\varphi = 30^\circ$ and 60° the approximation yields also good results for the length of the detection area depending on the electrical attenuation (Figure 13).

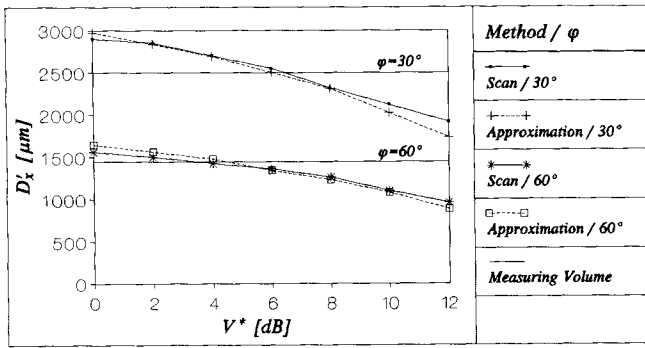


Fig. 13: Length D_x' of the detection area versus electrical attenuation V^* for $\varphi = 30^\circ$ and 60° off-axis measurements at a steel bead with the APD-receiver. The results were obtained from the scan measurements and the period method (approximation).

This is shown by the small deviations between the measured (scan) and the calculated (approximated) values. Further, it is remarkable that these results were obtained with relatively long measuring volumes. For $\varphi = 60^\circ$ the ratio $D_p'/D_x'/\sin\varphi$ was 0.25 and for $\varphi = 30^\circ$ it was 0.44.

4.1.4 X-coordinate, Refraction

The approximation for the length of the detection area, discussed in the previous section for reflecting particles, was also applied to measurements with refracting water droplets. Analogous to the measurements with the steel bead, the experimental investigations with monodisperse water droplets were performed with 30° and 60° off-axis instrument configurations. In order to reduce the size range, the beam intersection angle of the transmitting system and the focal length of the receiving system were changed, resulting in a reduction in the length of the measuring volume nearly by half. The measurement results are shown in Figure 14.

The differences between the scan results and the approximated values are not as small as for the measurements with the steel bead, which was relatively large in comparison with the water droplets ($d = 55 \mu\text{m}$).

The errors i.e. the differences between the results of the different types of evaluation, increased about 11%, which may have been caused by the reduced signal-to-noise ratio leading to erroneous period counting. Moreover, small trajectory displacements of the water droplets contribute to these deviations.

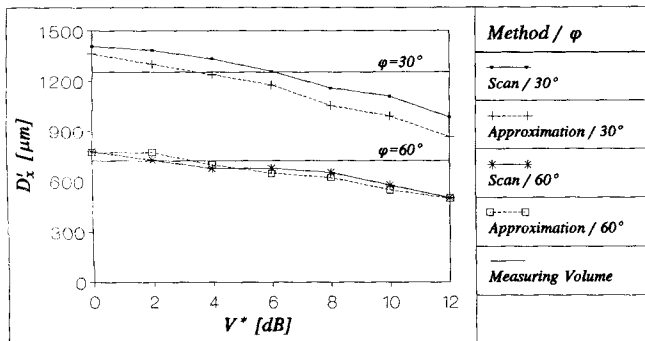


Fig. 14: Length D_x' of the detection area versus electrical attenuation V^* for $\varphi = 30^\circ$ and 60° off-axis measurements at water droplets ($d = 55 \mu\text{m}$) with the APD-receiver. The results were obtained from the scan measurements and the period method (approximation).

4.2 Polydisperse Particles

The particle size distributions measured with a 30° off-axis PDA and with different instrument sensitivities (electrical attenuations) are shown in Figure 15 in form of the particle rate n (per 60 s). It is obvious, that the reduction in the sensitivity is followed by a reduction in the particle rate, especially for small particles. This is equivalent to a “shift” of the distributions to larger particle diameters, because the instrument is not sensitive enough to detect small particles, which is also verified calculating the minimum detectable/measurable particle diameter d_{min} by means of Eq. (19).

For the graph in Figure 16 and also for calculating the dimensions of the detection area according to Eq. (16) and Eq. (20), the necessary parameters d_0 and N_0 of the reference particle were obtained in situ from the actual measurement. The in situ determination of one reference particle was done in such a way as to guarantee that this particle crosses the detection area in its centre, perpendicular to the interference planes with maximum probability. Therefore, that size class with the maximum number of particles was considered as the reference class and that particle in the reference class which produced the maximum number N_0 of burst periods was defined as the reference particle with diameter d_0 .

Comparing the lower ends of the measured particle size distributions in Figure 15 with the calculated minimum detectable particle diameter d_{min} in Figure 16, it is conspicuous that particle diameters below the corresponding lower limits, calculated by Eq. (19), were measured. This broadening of the particle size distribution is caused by erroneous signal processing due to low signal-to-noise ratios.

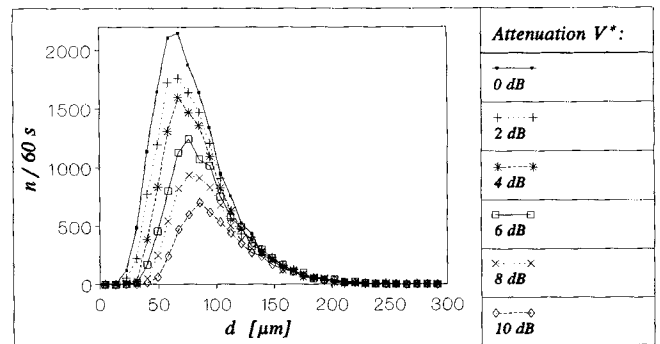


Fig. 15: Particle rate n in dependence on the particle diameter d for different settings of the electrical attenuation V^* (instrument sensitivity) measured with the APD-receiver in the spray cone of a pressure atomizer ($\varphi = 30^\circ$).

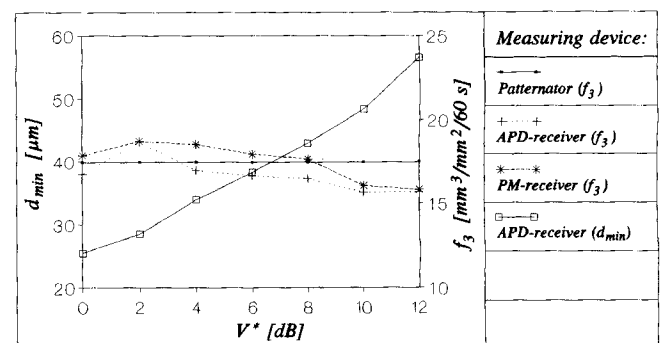


Fig. 16: Calculated lower limit d_{min} of the size range for the measurements described by Figure 15 and the volume flux densities f_3 , measured with different devices ($\varphi = 30^\circ$).

Before the procedure of weighting can be applied to the measured size distributions, and before volume flux densities or other parameters can be determined, all events which were not accepted by the signal processing must be distributed among those size classes which are not empty. One possibility for an appropriate procedure can be gathered from the measurements with steel beads.

The graph in Figure 17 shows a typical example of the distribution of those events which could not be validated by the signal processing system. As already shown in Figure 11, even along the x -axis the size limitations of the detection area are caused by a reduced signal strength, which again results in decreased signal-to-noise-ratios (SNR). For this reason, these signal processing errors are preferably detected if the particles pass through the cross-sectional area of the interference volume or through the x - y coordinate plane at the borders of the detection area or in its vicinity. Although this result was obtained from a measurement with a steel bead, it can also be used to give an explanation for rejecting signals. Therefore, the inferences will be applied to measurements with water droplets.

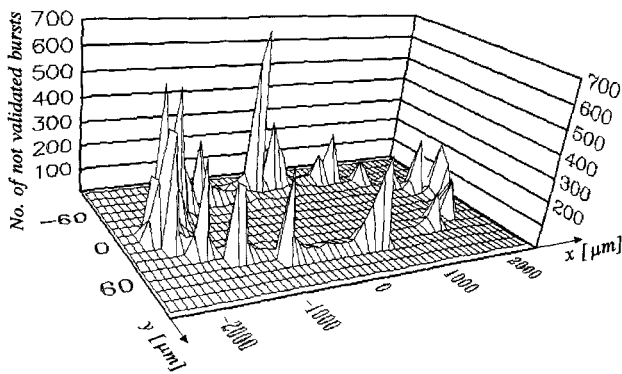


Fig. 17: One example of the distribution of not validated bursts in the detection area and its vicinity. The corresponding measurement was conducted with a reduced number of positions and an increased number of attempts.

Consequently, all the particles producing non-evaluable bursts are distributed among the particle size classes in a way that the increase in particle numbers is proportional to the length of the circumference of the detection area of each individual size class in addition to being weighted with the share of particles in the corresponding size class. Further, this procedure of distributing rejected events can only be performed for particles with diameters exceeding the lower limit d_{\min} .

In principal, the difficulties due to the low SNR (e.g. broadening of size distributions and high rejection rates) can be overcome by using improved methods and hardware for signal detection and signal processing based on, e.g., Fourier transform. In the present investigations this could not be realized. After this correction of the measured particle size distribution, the weighting can be performed and all parameters of interest, e.g. mean values and flux densities, can be determined. For the present investigations, the volume fluxes are of special interest. The volume flux densities f_3 , also shown in Figure 16, are given by

$$f_3 = \frac{\pi}{6T_M} \sum_{i=1}^{36} \frac{n(d_i) d_i^3}{A(d_i)} \quad (21)$$

where T_M = measuring time, A = area of detection and d_i = centred particle diameter of size class i . The results were

measured with two different types of receiver at a 30° off-axis position and they can be compared with patternator results. In the case of high instrument sensitivities ($V^* \leq 6-8$ dB) all results are in relatively good agreement, but at higher attenuations the lower limit d_{\min} of the size range becomes too large, causing a decrease in the corresponding number distribution and lower volume flux densities. In the appropriate range of sensitivity the deviations do not exceed a 7% margin, which is a comparatively good result.

Apart from volume flux densities, the procedure of weighting was analysed by means of the number distributions. It was not possible to apply a reference measuring technique to obtain local number distributions of particle sizes. For that reason, the particle size distributions measured with different off-axis arrangements of transmitting and receiving optics were compared with each other. In this context it is important only to compare measurements conducted with nearly the same sensitivity, which means that the parameter d_{\min} of the corresponding measurements must be nearly equal, otherwise the weighted distributions will be not comparable because they are very different at small particle diameters. The effect of weighting on the measured size distribution is shown in Figure 18.

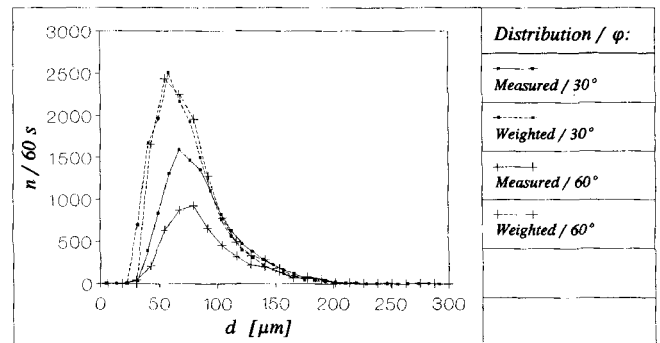


Fig. 18: Comparison of measured and weighted particle rates in different size classes for two off-axis angles ($\phi = 30^\circ$ and 60°).

Although the measured particle rates and the sizes of the detection areas for 30° and 60° off-axis instrument configurations are very different, the procedure of weighting yields almost the same size distributions.

4.3 Errors

For all types of measurements presented in the previous sections, the most important error source is the period counting, performed by the counter processor. Even in the case of high signal qualities and high SNR, an error of at least ± 1 period at each end of the bursts must be considered, which means that the counting of the maximum number of periods N_0 can be performed with an accuracy of ± 2 periods. These absolute errors may cause relative errors of more than about 15% with respect to the diameters of the detection area, which moreover can increase with decreasing SNR, which depends primarily on the particle size and the surface roughness of the particle in the case of constant instrument sensitivity. Apart from the counted number of periods N_0 , the resultant relative error is influenced by the ratio N_0/N_f . Consequently, the configuration of the transmitting system, which generates the interference volume with N_f fringes, can further influence the accuracy of the determined size of the detection area.

In order to reduce the errors combined with the period counting, the burst length measurement should be performed with a higher resolution, for instance by means of a time measurement from the beginning to the end of each burst. Since this was not possible with the counter used for the experimental investigations, the statements concerning the precision and the extensions of the detection area are limited to these preconditions. In connection with the measurements of monodisperse particles, further errors, caused by inaccuracy of the positioning devices, could be considered, but this is omitted because the deviations between the different measuring methods can be explained exclusively by the uncertainty of counting the burst periods. For the same reason the errors of the patternator measurement results were not analysed.

5 Summary

Improved results with respect to the size of the detection area of a PDA obtained by empirical and analytical considerations have been presented. Both the width and the length of the detection area are described by the burst length and by the number of signal periods. This means that in addition to the width, the length of the detection area also is not constant. Consequently, in contrast to former assumption, it is not identical with the length of the measuring volume, which is defined by the image of the aperture of the receiving optics, even if the measuring volume is very small in comparison with the interference volume.

By means of experimental investigations with monodisperse particles concerning the dependence of the size of the detection area on the particle diameter, the instrument sensitivity and the instrument configuration, the theoretical results could be verified. Further, there were no significant differences between the results obtained from reflecting steel beads and from refracting water droplets. The maximum errors of about 11 % in the case of small particle diameters could be reduced in future by a more precise burst length measurement instead of the applied period counting with low resolution.

The results for the size of the detection area were also for an in situ weighting of particle size distributions, measured in the spray cone of a pressure atomizer. The comparison of the calculated volume flux density with additional patternator measurement results showed only small deviations, which can also be explained by erroneous period counting. Apart from this, the weighting procedure was verified by measurements of the size distributions, because after applying the weighting procedure, being based on the area of detection, the original different distributions became nearly identical.

6 Symbols and Abbreviations

A	area of detection
C, C_1	constants
d	particle diameter
d_i	centred particle diameter of size class i
d_0	diameter of a reference particle
d_{\min}	minimum measurable particle diameter
D^*	normalized diameters of the effective measuring volume
D_L	diameter of laser beam
D_x, D_y, D_z	$1/e^2$ intensity diameters of the interference volume
D'_x, D'_y	diameters of the effective measuring volume
D_p	width of the slit or pinhole aperture in the receiving system

D'_p	width of the magnified aperture
f_3	volume flux density
f_b	burst frequency
f_s	shift frequency
I^*	normalized intensity
I_0	maximum intensity (in the centre of a laser beam)
I_P	incident light intensity on the particle
I_S	scattered light intensity
n	particle rate
N_0	number of burst periods from a reference particle without offset
N_b	total number of burst periods including frequency offset
N_f	number of fringes in the interference volume
N_{\max}	maximum number of signal periods
N_{\min}	minimum number of signal periods for validation
N_S	additional number of burst periods due to frequency shift
P_P	incident light power on the particle
P_S	scattered light power
T_M	measuring time
U	signal voltage
U_t	trigger level
V	electronic amplification
V^*	electrical attenuation
x, y, z	cartesian coordinates
θ	half beam intersection angle
λ	wavelength of laser light
φ	off-axis angle

7 References

- [1] *K. Bauckhage, H.-H. Flögel*: Simultaneous measurement of droplet size and velocity in nozzle sprays. Proc. 2nd Int. Symp. on Applications of Laser Anemometry to Fluid Mechanics, Lisbon, Portugal, 1984, July 2–4.
- [2] *M. Saffman, P. Buchhave, H. Tanger*: Simultaneous measurement of size, concentration and velocity of spherical particles by laser Doppler method. Proc. 2nd Int. Symp. on Applications of Laser Anemometry to Fluid Mechanics, Lisbon, Portugal, 1984, July 2–4.
- [3] *W. D. Bachalo, M. J. Houser*: Phase-Doppler spray analyzer for simultaneous measurements of drop size and velocity distributions. Opt. Eng. 23 (1984) 583–590.
- [4] *F. Durst, M. Zaré*: Laser-Doppler measurements in two-phase flows. Proc. of LDA Symp., Copenhagen, Denmark, 1975, pp. 403–429.
- [5] *W. D. Bachalo, M. J. Houser*: Spray Drop Size and Velocity Measurements using the Phase/Doppler Particle Analyzer. Proc. Int. Conf. on Liquid Atomization and Spray Systems (ICLASS), London, GB, 1985, July 8–10.
- [6] *K. Bauckhage*: The Phase-Doppler-Difference-Method, a New Laser-Doppler-Technique for Simultaneous Size and Velocity Measurements – Part 1: Description of the Method. Part. Part. Syst. Charact. 5 (1988) 16–22.
- [7] *K. Bauckhage, H.-H. Flögel, U. Fritsching, R. Hiller*: The Phase-Doppler-Difference-Method, a New Laser-Doppler-Technique for Simultaneous Size and Velocity Measurements – Part 2: Optical Particle Characteristics as a Base for the New Diagnostic Technique. Part. Part. Syst. Charact. 5 (1988) 66–71.
- [8] *K. Bauckhage, H.-H. Flögel, F. Schöne*: Size and Velocity Measurements of Spherical Particles in Multiphase Flows and the Prediction of Absolute Particle Concentrations. Int. Symp. on Optical Particle Sizing: Theory and Practice, I.N.S.A. de Rouen, France, 1987, May 12–15.
- [9] *M. Saffman*: Automatic calibration of LDA measurement volume size. Appl. Opt. 26 (1987) 2592–2597.
- [10] *W. D. Bachalo, R. C. Rudoff, A. Breña de la Rosa*: Mass Flux Measurements of a High Number Density Spray System Using the Phase Doppler Particle Analyzer. AIAA 26th Aerospace Science

- Meeting, Reno, Nevada, 1988, Jan. 11-14, Paper No. AIAA-88-0236.
- [11] *F. Schöne, K. Bauckhage, T. Wriedt, D. Bergmann, T. Evers*: Experimental investigations on the size of the measuring volumes of different backscatter phase-Doppler-anemometers. Fourth Int. Conf. Laser Anemometry, Advances and Applications, Cleveland, Ohio, 1991, Aug. 5-9, pp. 637-643.
- [12] *M. Sommerfeld, H.-H. Qiu*: Particle Concentration Measurements in Complex Two-Phase Flows using Phase-Doppler-Anemometry. Prepr. 5th Europ. Symp. on Particle Characterization, Nürnberg, Germany, 1992, March 24-26, pp. 293-308.
- [13] *G. Gréhan, G. Gouesbet, A. Naqui, F. Durst*: Trajectory Ambiguities in Phase Doppler Systems: Use of Polarizers and Additional Detectors to Suppress the Effect. Proc. 6th Int. Symp. on Applications of Laser Techniques to Fluid Mechanics, Lisbon, Portugal, 1992, July 20-23.
- [14] *S. V. Sankar, A. S. Inenga, W. D. Bachalo*: Trajectory Dependent Scattering in Phase Doppler Interferometry: Minimizing and Eliminating Sizing Errors. Proc. 6th Int. Symp. on Applications of Laser Techniques to Fluid Mechanics, Lisbon, Portugal, 1992, July 20-23.
- [15] *W. D. Bachalo, A. Breña de la Rosa, S. V. Sankar*: Diagnostics for Fuel Spray Characterization, in *N. Chigier* (ed.): Combustion Measurements. Hemisphere Publ. Corp., 1991, pp. 229-278.
- [16] *R. W. Sellens*: Alignment Errors in Phase Doppler Receiving Optics. Part. Part. Syst. Charact. 7 (1990) 116-120.
- [17] *U. Manasse, Z. Jiang, T. Wriedt, K. Bauckhage*: Application of the Phase Doppler Technique to Optically Absorbent Liquids. Int. Conf. Particle Size Analysis, Loughborough, U. K., 1991, Sept. 17-19.
- [18] *A. Naqwi, X. Liu, F. Durst*: Dual-Cylindrical Wave Method for Particle Sizing. Part. Part. Syst. Charact. 7 (1990) 45-53.
- [19] *M. Dannehl, G. Schulte*: Experimental Results of the Investigation into the Two Phase Flow and Air Entrainment in the Spray Cone of an Atomizer Obtained by the Phase-Doppler-Method. Proc. 4th Int. Symp. on Applications of Laser Anemometry to Fluid Mechanics, Lisbon, Portugal, 1988, July 11-14.